Solid Freeform Fabrication 2023: Proceedings of the 34th Annual International Solid Freeform Fabrication Symposium – An Additive Manufacturing Conference
Reviewed Paper

EMBEDDING TEMPERATURE SENSORS WITH THE USE OF LASER-FOIL-PRINTING ADDITIVE MANUFACTURING

T. Turk[1], M. Dougan[1], L. Hendrix[1], A. Reed[1], C. E. Dominguez[2], A. T. Sutton[2], J. Park[1], and M. C. Leu[1]

[1]Department of Mechanical and Aerospace Engineering, Missouri University of Science and Technology, Rolla, MO 65409
[2]Los Alamos National Laboratory, Los Alamos, NM 87545

Abstract

Laser foil printing (LFP) is a metal additive manufacturing (AM) process using laser-based melting of metal foil technique. Using metal foils in AM has advantages over laser powder-feed processes, allowing for efficient heat transfer and resolving the drawbacks of powder-based AM such as potential powder inhalation health hazards, balling, spattering, and high powder costs. In this study, we demonstrate the advantage of LFP for embedding sensors into structures using 304L stainless-steel foil as the feed material and two different types of temperature sensors. The first type is a resistance temperature detector (RTD) platinum sensor (Pt 100), and the second type is a k-type thermocouple probe. A detailed study of the sensor embedment through LFP revealed that the spot-welding scanning strategy significantly improves the product quality than conventional line-welding scanning strategy. As a result of this study, the feasibility of fabricating functional parts with embedded sensors using the LFP process is demonstrated.

Introduction

According to the American Society for Testing and Materials (ASTM), AM is a general term for successfully joining materials layer-by-layer to form 3D parts, which is different from the traditional subtractive and formative manufacturing technologies [1]. There are a wide variety of AM techniques and categorization is based on the process architecture and characteristics. The following are the seven general AM categories [1]: binder jetting (BJT), directed energy deposition (DED), material extrusion (MEX), material jetting (MJT), powder bed fusion (PBF), sheet lamination (SHL), and vat photopolymerization (VPP). Two of these categories are similar to the process used in this study, laser foil printing (LFP), although it is not categorized in ASTM due to its unique processing technique. Sheet lamination (SHL) is a category that uses sheet/foil feed but fuses the layers using ultrasonic consolidation or adhesive joining. Directed energy deposition (DED) uses wire/powder feed, laser/electron beams, or electric arc to melt the feed material selectively. Laser foil printing (LFP) uses laser beams to melt the feed material of metal foils selectively. Therefore, the method of LFP does not fall directly under one of the seven AM categories, but it is somewhere between sheet lamination (SHL) and directed energy deposition (DED).

Since LFP was invented at Missouri University of Science and Technology [2], [3], some materials applications, characterization, and automation studies have been researched. As

examples, aluminum 1100 alloy [4], AISI 1010 low carbon steel alloy [3], 304L stainless steel alloy [5], [6], and zirconium-based amorphous metal [7]–[10] are material applications researched with the use of LFP. In addition, a comparative study between LFP and a commonly used laser powder bed fusion (LPBF) technology revealed that the finer grain structure and lower porosity of the laser-foil-printed part resulted in higher strength [6]. Moreover, the fast-cooling rate of LFP helps to form amorphous metal parts, which are difficult using other AM technologies and traditional manufacturing processes [7]–[10]. Most recent studies focused on automating the LFP system [11], [12] and improving process productivity with parameter optimization and laser polishing experiments [13].

In the present study, we experimentally investigate the feasibility of sensor embedding using LFP additive manufacturing. The utilization of embedded sensors is gaining increased traction in both industrial and academic circles. To provide an example, the demands of Industry 4.0 encompass the integration of Internet of Things (IoT) technology featuring embedded sensors, applied across supply chain management, automated manufacturing, and complementary operational systems [14]. In addition, the sensors can be used for structural health monitoring via embedded sensors to obtain strain, residual stress, and temperature variations during the component's lifecycle [15]. As a consequence of the layer-by-layer approach inherent in AM, these processes serve as more practical fabrication methods when compared to conventional manufacturing strategies for enclosing sensors into desired parts, such as capacitors, thermal and pressure sensors, resistors, microchips, structural electronics, and many others [16]. The design concepts of embedding the electronic components into metal parts for the LPBF process are presented in the research paper by Binder et al.[17], where they demonstrated that a weldable strain sensor could be embedded into a nickel alloy IN718 metal part by this process [18]. However, the use of a powder bed in the LPBF process makes the application of sensor embedding highly challenging. Specifically, the process needs to be interrupted, the powder in the printed housing groove removed, and then the sensor placed during the embedding [19]. Moreover, process-related defects and anomalies such as keyholing, balling, and spattering are commonly known drawbacks of using powder-bed AM [20]. Additionally, Nunez et al. presented the embedment of thermocouples with DED [21]. The results showed that processing defects and porosities can be present, and the embedment strategy is critical. DED applications also include some hybrid processes using subtractive techniques[22] and ceramic deposition [23] to avoid defects to have improved surface quality and lower porosity. Yet, combining different processes would add additional steps and lower productivity. Another application for embedding functional parts is Ramanathan's research of piezoelectric polyvinylidene fluoride (PVDF) sensor embedding using ultrasonic additive manufacturing (UAM) [24]. UAM typically uses a milling operation to form the desired geometry and consolidates the sheets to form parts [25]. LFP uses a clean atmosphere without dust or unmelted powders in the formed grooves for embedding geometries, does not include any machining operation, and fully melts the foil feed resulting in dense metal parts with fine grain structure. On the other hand, LFP can also have high thermal loadings that can cause part defects and damage the embedded component during processing. In specific, foil welding has a lower spatter risk than powder welding. This is because the molten metal is less likely to be ejected from the weld pool when welding foil. However, optimized scanning strategies can mitigate the drawback of potential processing issues. As a result, LFP can be a practical approach for embedding sensors and other types of electronic components into metallic parts.

The main objective of this study is to investigate the feasibility of embedding components into metal parts using LFP process. To showcase the potential of LFP for sensor integration with the capability of in situ measurements, temperature sensors have been selected as the components for demonstration purposes. This research aims to demonstrate how LFP can effectively embed sensors within metal parts during fabrication without damaging the sensor and the evidence of thermal decay.

Overview of LFP process steps and system

The LFP system consists of a continuous-wave (CW) infrared (IR) fiber laser for welding, and an ultraviolet (UV) pulsed laser for excess foil removal. The CW laser (IPG YLR-1000-MM-WC-Y11) subsystem includes a galvo mirror scanner (SCANLAB hurrySCAN 30) and an f-θ lens. The CW fiber laser has a center wavelength of 1070 nm, beam quality factor M^2 of 3.04, and maximum average power output of 1000 W. The focal length of the F-θ lens is 330 mm, and the laser spot size is 160 µm. The UV pulsed laser (Coherent AVIA-355X) subsystem includes optical reflection mirrors and a focal lens. The UV laser's center wavelength is 355 nm, the pulse width is 30 ns, and the maximum average power output is 10 W. The focus length of the lens is 100 mm, and the laser spot size is 40 µm. Both the CW and UV laser beams are focused on the foil surface. In addition to the dual laser system, a 3-axis gantry system moves the specimen between the cutting laser and the welding laser. A circularly perforated foil clamping plate is used to apply pressure on the foil to hold the feed foil in place during the spot-welding step. A roller-to-roller foil supplier and a mechanical polisher are other system sub-components. Figure 1 shows the automated LFP system developed.

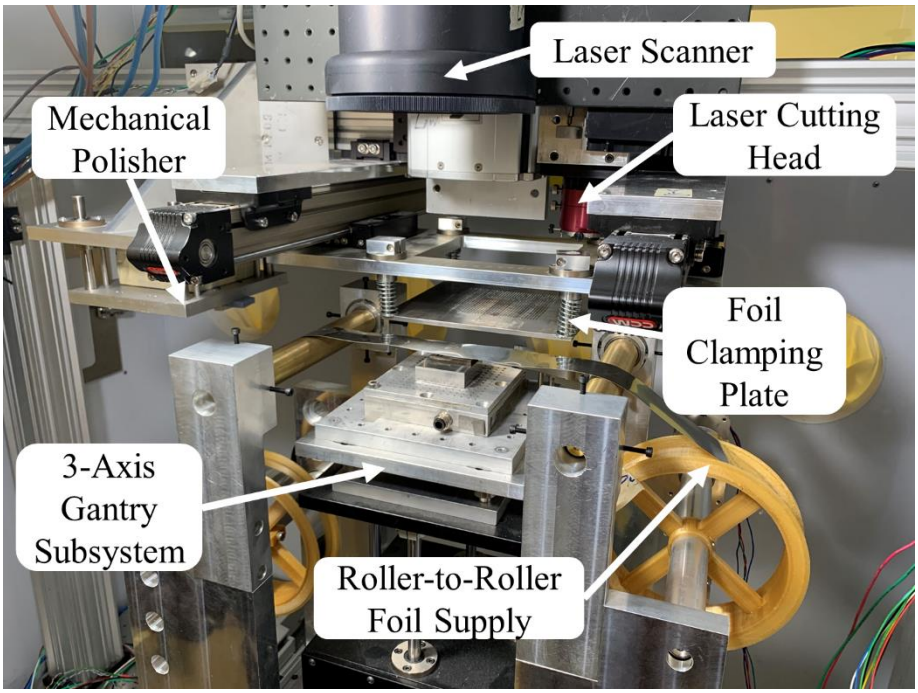

Figure 1: In-house developed automated LFP system. [11]

LFP is a metal AM process to build a part via selective laser fusion of sheet feedstock material to a substrate. The LFP has multiple steps of (1) spot welding, (2) pattern welding, (3)

contour cutting, and (4) edge polishing all of which are schematically shown in Figure 2. Spot-welding step is the first step, and the foil clamping plate is used to compress the foil feed with the attached springs. Thus, spot-welding provides an attachment of the foil to the previous layer/substrate to prevent thermal distortion of the feed foil during the next step of pattern welding. In pattern welding, the material layer bonding occurs via the complete melting of the foil material. Then, contour cutting takes place to remove excess foil by detaching the layer from the feed. During UV cutting, burrs are produced; any non-flat surface features would result in defective welding for the following layer. Therefore, the final step is edge polishing to remove the burrs and flatten the part surface with a mechanical polisher consisting a #80 grit aluminum oxide grindstone.

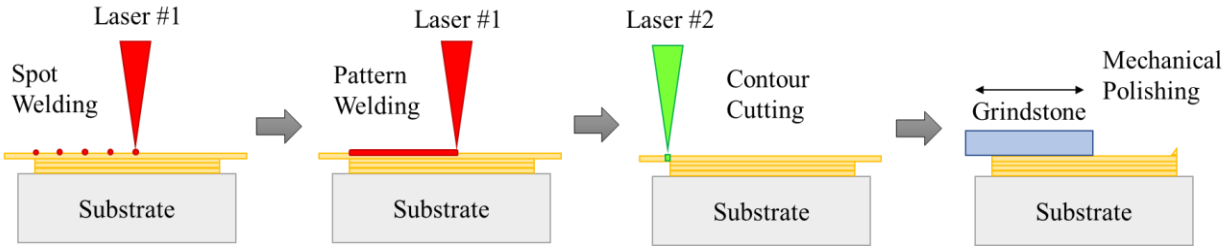

Figure 2: Illustration of the current process steps of LFP. From left to right: spot welding, pattern welding, contour cutting, and edge polishing. [11]

Types of sensors in the embedding experiments

The most common types of thermal sensors are thermocouples, mercury/alcohol thermometers, resistance thermometers, and radiation thermometers [26]. For demonstration we selected two different types of thermal sensors: thermocouples and resistance-based thermometers. Resistance thermometers, also known as resistance temperature detectors (RTDs), are made of pure material, such as platinum, to measure and calculate the temperature based on a linear relationship [26]. Thermocouples are composed of two metals to create a voltage between the hot sensor element and the cold reference junction [26]. Typically, thermocouples are less accurate than platinum RTDs, but the temperature range of measurement for thermocouples can be wider depending on the material type [26], [27]. The other considerations may include service life, the effect of pressure or vacuum, thermal decay or survival, and the thermal sensor cost in application [27].

The advantage of LFP for embedding sensors into structures are demonstrated using 304L stainless-steel foil as the feed material due to its availability and ease of welding. This foil purchased from Ulbrich Stainless Steels & Special Metals Inc. has a thickness of 0.005 inches (0.127 mm). Among the alternatives of temperature sensors available from the market, we selected two different types of sensors. The definitions, sensor types, dimensions, and temperature ranges for the two options are given in Table 1. The first sensor is an RTD, and it is selected because of its compactness and flatness facilitating embedment. It was purchased from the Innovative Sensor Technology IST AG with the product code 100513. The second sensor was selected because it has a weld pad, which allows LFP to perform laser welding onto the metal pad. It was purchased from Harold G. Schaevitz Industries LLC with the product code WPTC-ST-04-072-K-N. These two sensors with the cable and wiring assemblies are shown in Figure 3.

Table 1: Temperature sensor information

#	Definition	Sensor Type	Dimensions	Temperature Range
1	Pt100, IEC 60751 F0.3 for high temperatures	RTD	5 x 1.6 x 0.65 [mm]	-200 to +750 [°C]
2	WPTC weld pad surface temperature thermocouple probe	K-Type	25 x 25 x 0.25 [mm] (Pad dimensions)	-100 to +1300 [°C]

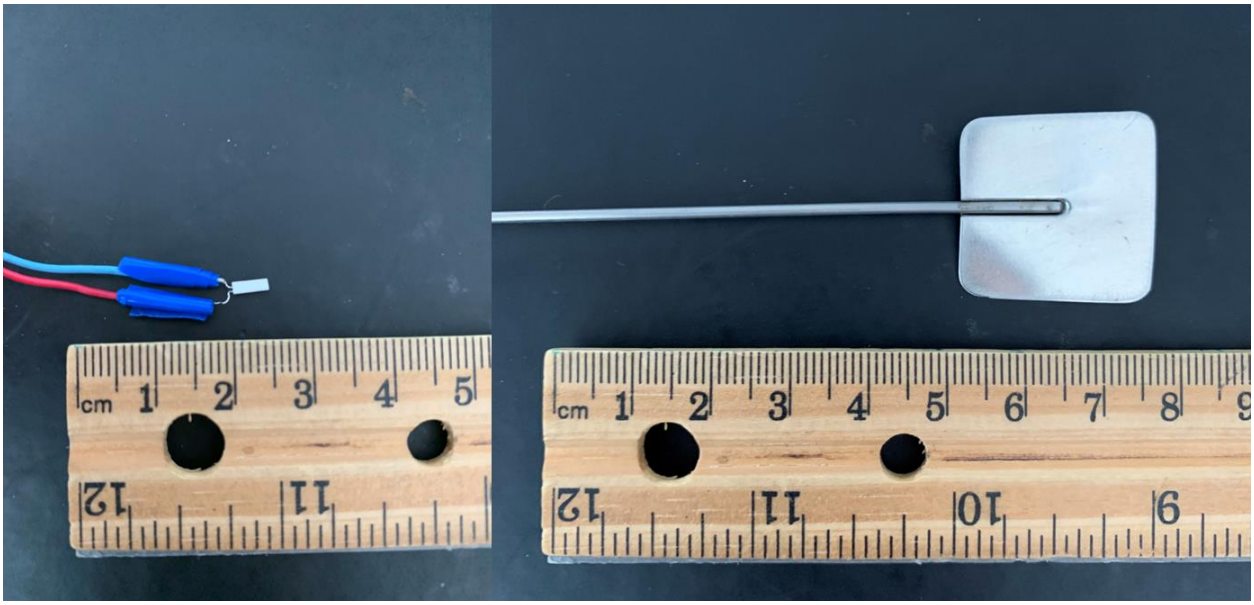

Figure 3: Pt100 RTD sensor (left) and weld pad thermocouple (right).

Spot welding as a scanning strategy

In the previous studies of LFP, the common scanning strategy of line raster scanning technique was used for the pattern welding step. Thus, the initial printing experiments used this approach. However, this scanning strategy needs to have a parameter investigation study to determine the best laser scanning parameters. The results show that although the rectangular base plate could be printed successfully, printing a groove shape resulted in defects and unsuccessful printing, as shown in Figure 4. This is because the geometry of the groove shape has thin walls, which has a much slower cooling rate than the rectangular plate, leading to some heat accumulation and resulting in foil distortion and the Marangoni effect. Therefore, a strategy of dense spot welding is investigated during the pattern welding step.

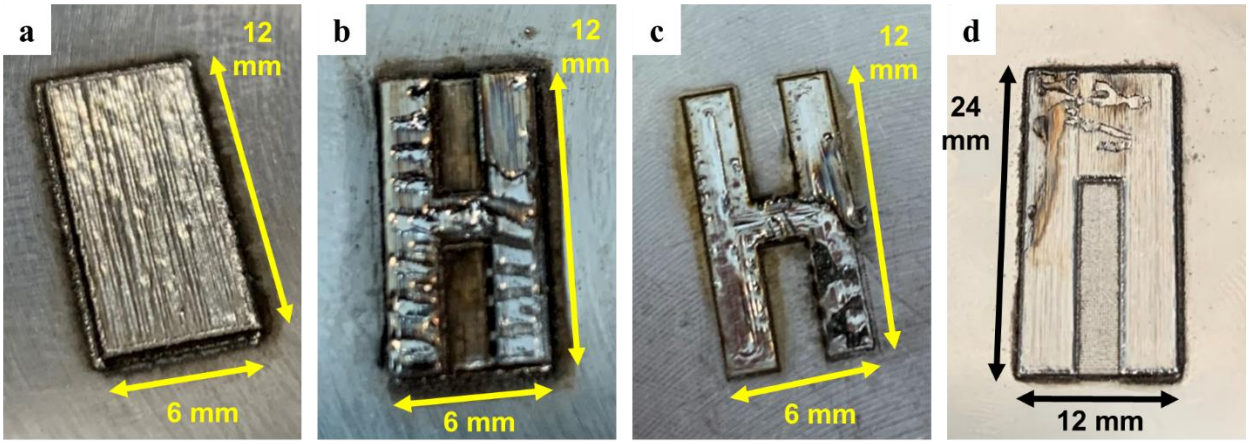

Figure 4: Sample printing results: (a) successful prints for a rectangular plate, (b-c) defective surface for the H-shape of Pt100 RTD, and (d) defective surface for the groove shape of WPTC.

Spot scanning strategy is the application of laser welding discretely, which is different from continuous laser raster line scanning, see Figure 5. Calculations were done to determine the processing parameters for laser spot welding. According to Hung et al. [6], volumetric energy input (VEI) of the welding modes can be calculated with the equations 1 & 2, where P is the laser power [W], v is the laser scanning speed [mm/s], h is the hatch space [mm], s is the layer thickness [mm], t is the dwelling time [s], and d is the distance between spots [mm]. According to another research on the LFP process [5], the best laser welding parameters obtained had a VEI of 104.98 [J/mm^3]. Thus, to achieve the same VEI, with 400 [W] laser power, 0.1 [mm] spot distance, 0.1 [mm] hatch space, and 0.127 [mm] layer thickness, laser dwelling time should be set to 0.333 [ms].

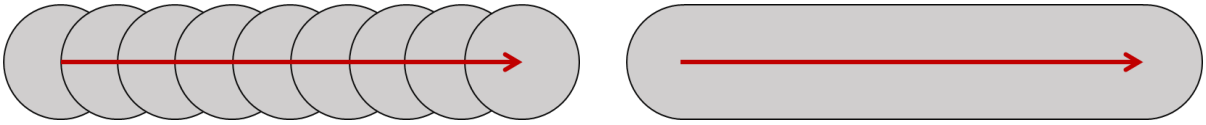
Figure 5: Illustration of spot scanning (left) and line scanning strategies (right).

$$VEI_{line} = \frac{P}{v \cdot h \cdot s} \quad (1)$$

$$VEI_{spot} = \frac{P \cdot t}{d \cdot h \cdot s} \quad (2)$$

The single energy input (SEI) for line and spot scanning are compared via theoretical calculations below. The length (l) of the scanned line varies between 1.6-24 [mm]. Thus, the following calculations include minimum and maximum single energy input for line scanning. The results show that the single energy input for the line scanning strategy is 16-240 times higher than the spot scanning respectively.

$$SEI_{line} = P \cdot \frac{l}{v} \quad (3)$$

$$SEI_{line-min} = 400\ W \cdot \frac{1.6\ mm}{300\ {}^{mm}/_{s}} = 2.133\ J$$

$$SEI_{line-max} = 400\ W \cdot \frac{24\ mm}{300\ {}^{mm}/_{s}} = 32\ J$$

$$SEI_{spot} = P \cdot t \qquad (4)$$

$$SEI_{spot} = 400\ W \cdot 0.333\ ms = 0.133\ J$$

Figure 6 shows the dimensions for the geometries for the RTD sensor, weld-pad thermocouple, and the scanning path for the dense spots. The spot-welding pattern used in this study is a contour pattern that starts from the edges. In a previous research study, scanning inward mitigates the risk of foil distortion during processing [13]. The reason is that linear scanning in one direction may cause foil distortion due to the heat accumulation towards one edge. The red dots in Figure 6 are the approximate sensor measurement locations. The locations are essential for analyzing and investigating the collected temperature variation data.

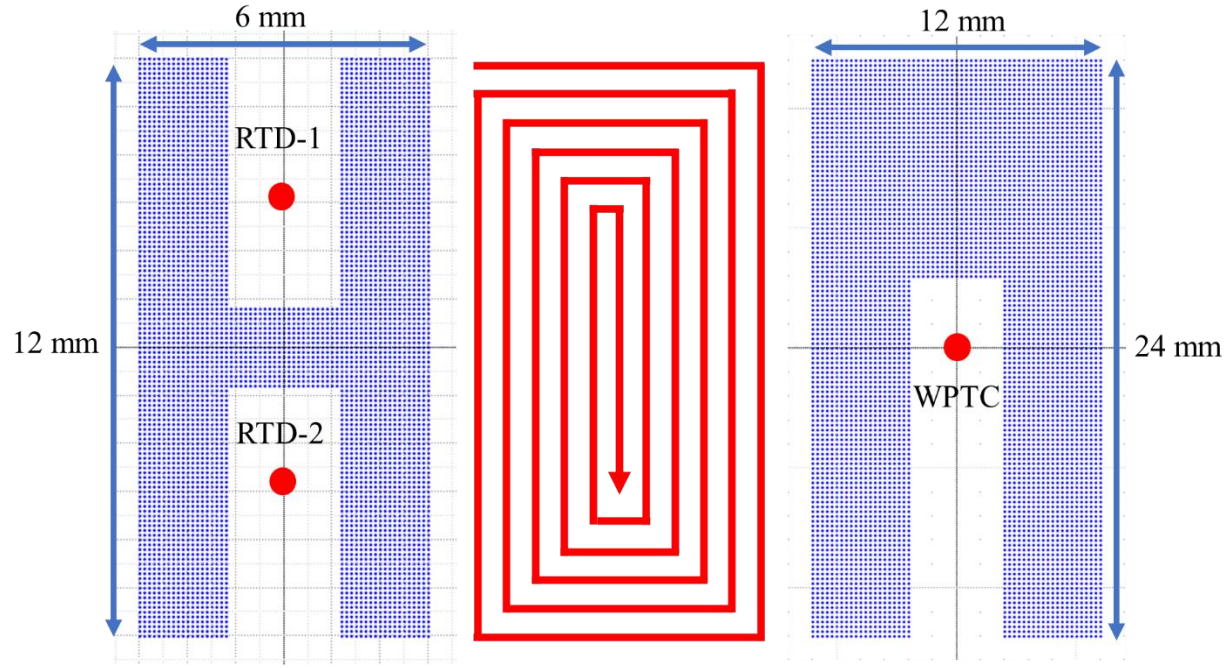

Figure 6: Dimensions of RTD sensor embedding geometry with sensor locations (left), contour pattern - spot welding path (center), and dimensions of WPTC sensor embedding geometry with sensor location.

Pt100 RTD sensor embedding

The laser-foil-printing experiments started with the computer-aided design of the Pt100 RTD sensor. First, the design files are prepared using SCANLAB laserDESK software, which is the laser processing software for the laser scanner used for welding. The sensor's compact size allowed for embedding two sensors in one assembly. Figure 7 shows the sensor and the double-sided design shape for embedding sensors.

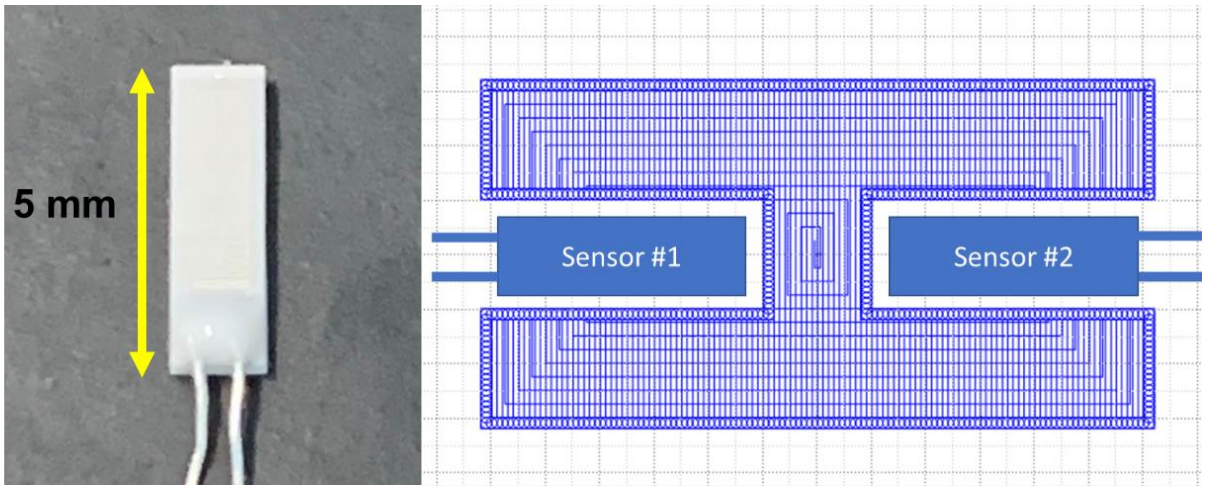

Figure 7: Image of Pt100 RTD sensor (left) and double-sided sensor embedding (right).

Printing started with the base rectangular plate and then continued additional layer printing of the grooved H-shape until the depth was tall enough to embed the sensors. Afterwards, we manually placed the sensors into the groove. Finally, another layer is printed on top of the sensors to complete the sensor embedding. The pictures of the sample are given in Figure 8.

Figure 8: Pt100 RTD embedding from left to right: grooved shape without sensors (first and second images), grooved shape with sensors, and after one layer printed on top of the sensors.

Embedding temperature sensors helps to investigate the LFP processing in terms of in-situ welding monitoring. The measurements were collected using a EXCELOG-6 Six Channel Handheld Temperature Data Logger for Thermocouples and RTDs. Figure 9 shows the temperature variation during the spot-scanning strategy. The oscillation is due to scanning being a contour path and the measured temperature increasing and decreasing accordingly. The scanning starts from the top edge, see Figure 6, where sensor 1 is closer to the melt pool, and the first peak in the sensor 1 measurement can be seen, then it cools down. Then the first peak in the sensor 2 measurement can be seen. This oscillation repeats until the entire surface is scanned.

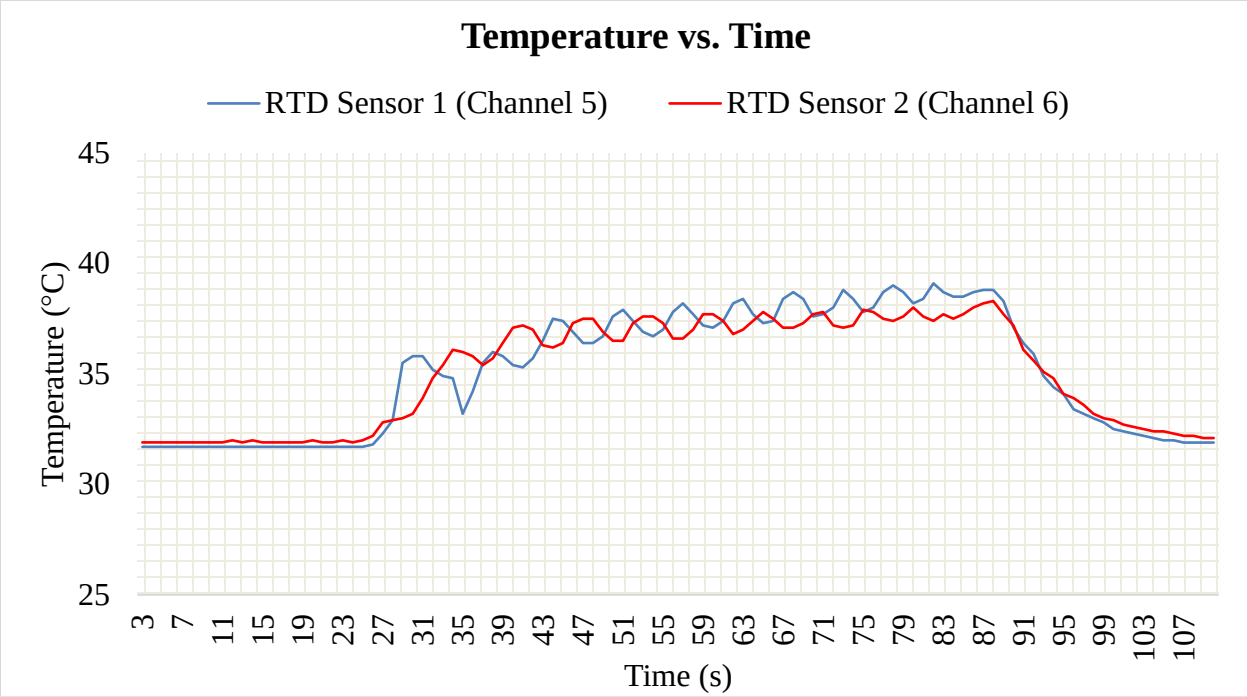

Figure 9: The plot of embedded Pt100 RTD sensor readings during the LFP processing.

Weld pad thermocouple (WPTC) embedding

After the study of embedding RTD sensors, embedding the second type of temperature sensor, i.e., the WPTC weld pad, was investigated. The embedding of this sensor started with its CAD model, which is shown in Figure 10 along with a photo of the sensor. Like the RTD sensors, the layer printing started with the base plate and continued with a groove shape with spot scanning. After the manual placement of the weld pad on top of the groove, the pad was welded on top of the surface of the previous layer. Then, the pad's exterior was cut using the UV cutting laser to maintain the rectangular geometry. The final layer printing on top of the sensor completed the embedding. Figure 11 and Figure 12 show the in-process LFP and sample pictures, respectively. As seen in Figure 11, the processing is done in argon gas shielding atmosphere to avoid oxidation.

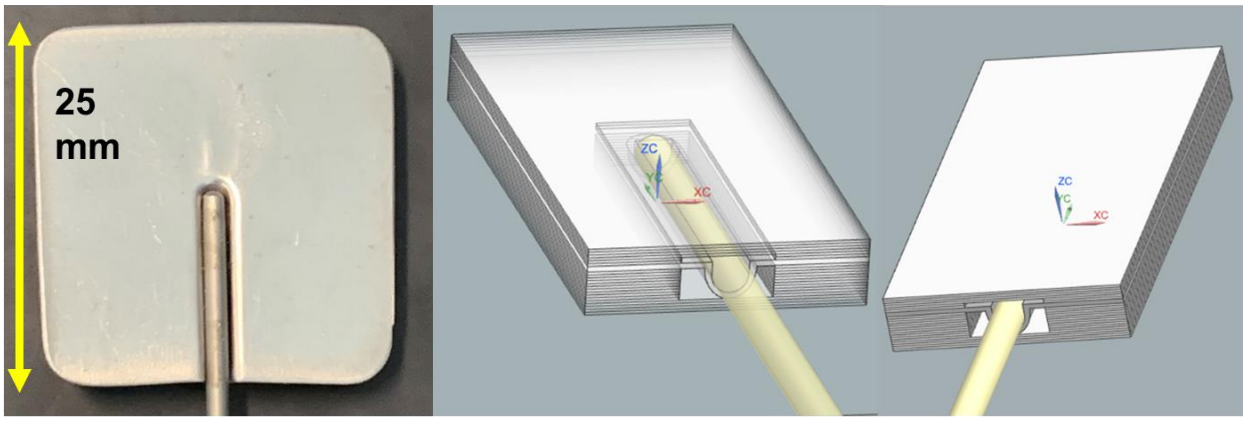

Figure 10: Images of WPTC weld pad (left), embedded WPTC weld pad with translucent layers (center), and embedded WPTC weld pad (right).

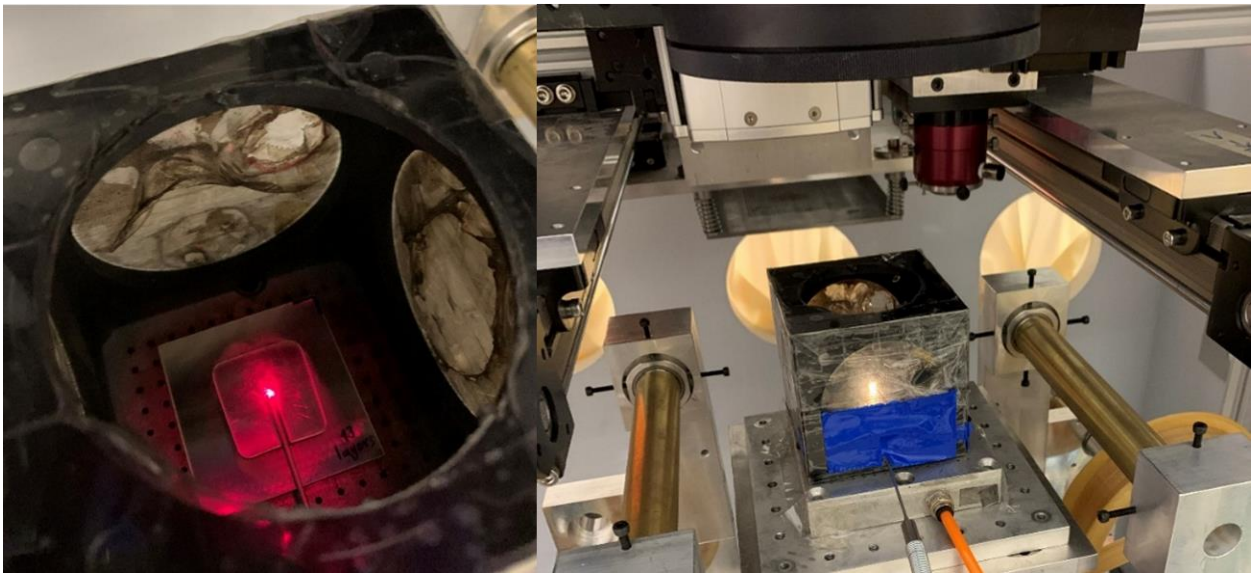

Figure 11: Laser foil printing of embedded WPTC: argon chamber assembly from top (left) and during spot welding (right).

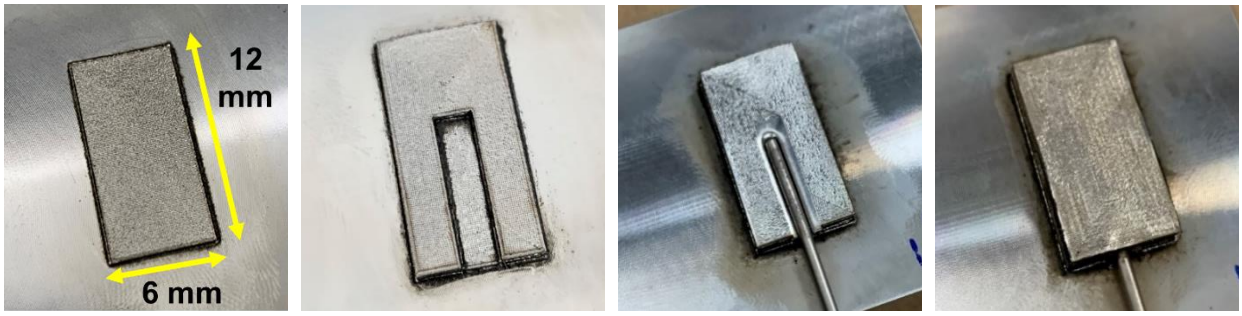

Figure 12: Weld-pad thermocouple embedding from left to right: printed base plate, grooved layers, welded pad after cutting, after printing another layer on top of the weld-pad.

The printing of the layer above the embedded sensor has also been monitored for in-process temperature variations, and the result is plotted in Figure 13. The overall temperature rises due to the repetitive laser energy input in the plot. However, it oscillates during the input due to the sensor location shown in Figure 6. During the scanning of the edges, the weld spots are closer to the sensor measurement location, causing the localized peaks, and the cooling down causes the troughs when the laser spot welding is applied to the top and bottom edges.

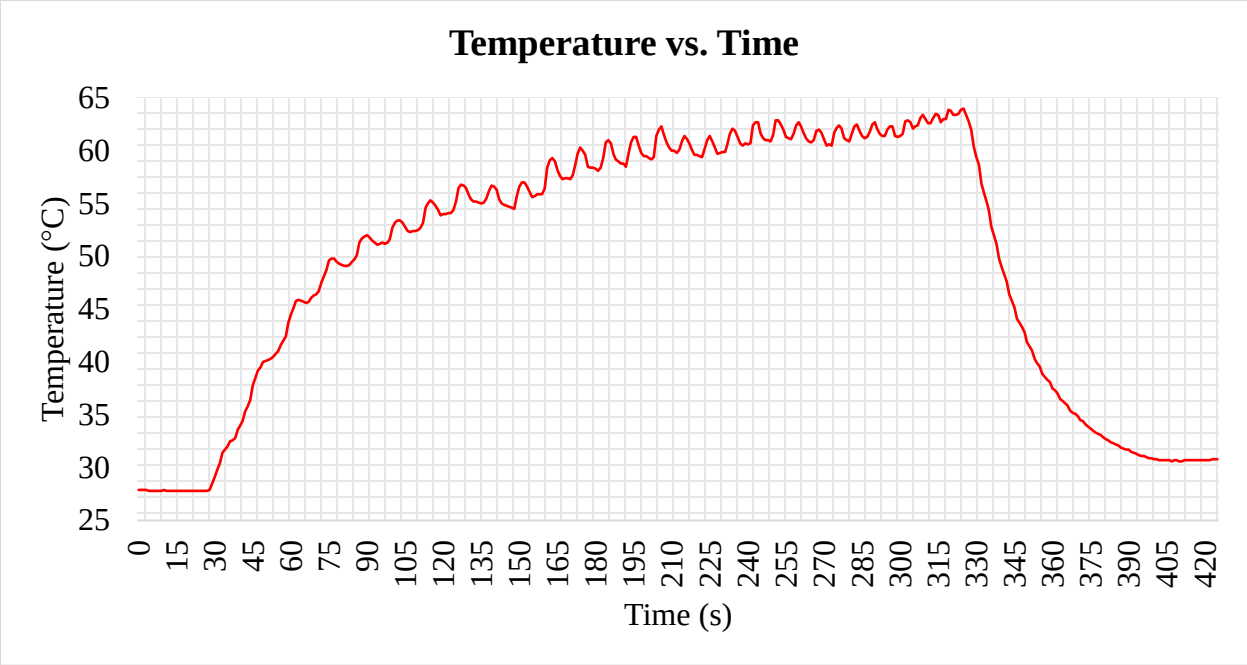

Figure 13: The plot of embedded WPTC readings during the LFP processing.

Discussion

In this initial study, two different types of temperature sensors are used to investigate the feasibility of component embedding into metal parts using the Laser Foil Printing (LFP) process. LFP has a clean fabrication environment and uses inexpensive metal foil as the feedstock, which is practical and cost-effective for sensor embedding purposes compared to popular powder bed metal AM techniques. This work showed that LFP is a viable means for embedding temperature sensors into metal parts. This can be further expanded to include strain and pressure sensors, electrical components, a wide range of different sensors, and many others.

During the sensor embedding experiments, various process parameters for pattern welding using line scanning resulted in defects due to thin walls and heat accumulation. Monitoring and simulation techniques have been used to predict processing-related defects and anomalies in metal AM processes. To ensure an accurate prediction, researchers use various process monitoring techniques including the use of pyrometers, infrared (IR) and charge-coupled device (CCD) cameras, and non-destructive testing (NDT) (computed tomography - CT and x-ray) [28], [29]. Numerical simulations use mostly finite element analysis with commercial software packages [30] or graph-theory approaches [31] to investigate the temperature field. LFP is a relatively new process that has yet to be analyzed using monitoring and simulations. In the spot-welding scanning strategy in this study, the single energy input is too low to heat up the entire part surface, which mitigates the potential processing-related defects. Also, the single energy input does not vary with part geometry, which is highly desirable for simulating the process and predicting its outcome. This scanning strategy has a high potential to avoid defects, but it needs further investigation into porosity, lack of fusion and/or delamination, mechanical properties, residual stresses, etc. in order to fully understand this technique compared with line scanning.

Temperature readings can be collected using the embedded sensor for in-process monitoring of the process employed to embed the sensor. As a result, the monitored temperatures are significantly lower than the melting temperature of 304L stainless steel, which is around 1450 °C. This is because the volume of melt pool is small using the scanning strategy of dense spot welding, allowing the part not to be heated entirely. Moreover, any risk of heat accumulation-related defects (keyholing, Marangoni effect, and many others) is mitigated. Nevertheless, when positioning the sensors within the designated design geometry, there exist clearance gaps of 0.2 [mm] on each side. These gaps lead to reduced conductivity between the sensor and the embedding material (stainless steel), potentially leading to decreased accuracy in temperature readings. The conduction rate between the sensor and the metal part can be increased by filling the gaps with high-thermal-conductive adhesives.

Conclusions

This study investigates the embedding of two different types of temperature sensors using laser-foil-printing (LFP) additive manufacturing. The first sensor is a resistance temperature detector (RTD), and the second is a K-type thermocouple probe. The process parameters in line scanning are crucial for printing successful parts with challenging geometries (e.g., thin walls) with embedding of sensors due to the high laser energy input. Therefore, an alternative scanning strategy is introduced in this paper: spot weld scanning. By using this scanning strategy, the successful embedding of these two temperature sensors into metal parts are demonstrated with thin-walled geometries using the LFP process.

Acknowledgment

This research work was partially supported by a research grant from the Los Alamos National Laboratory.

References

[1] ISO/ASTM, “ISO/ASTM 52900: Additive manufacturing - General principles - Terminology,” *International Standard*, vol. 5, pp. 1–26, 2015, [Online]. Available: https://www.iso.org/obp/ui/#iso:std:69669:en%0Ahttps://www.iso.org/standard/69669.html%0Ahttps://www.astm.org/Standards/ISOASTM52900.htm

[2] H.-L. Tsai, Y. Shen, Y. Li, and C. Chen, “Foil-based additive manufacturing system and method,” 2020 [Online]. Available: https://www.osti.gov/biblio/1771599

[3] C. Chen, Y. Shen, and H.-L. Tsai, “A Foil-Based Additive Manufacturing Technology for Metal Parts,” *J Manuf Sci Eng*, vol. 139, no. 2, Aug. 2016, doi: 10.1115/1.4034139.

[4] C.-H. Hung *et al.*, “Aluminum Parts Fabricated by Laser-Foil-Printing Additive Manufacturing: Processing, Microstructure, and Mechanical Properties,” *Materials*, vol. 13, no. 2, 2020, doi: 10.3390/ma13020414.

[5] C.-H. Hung, W.-T. Chen, M. H. Sehhat, and M. C. Leu, “The effect of laser welding modes on mechanical properties and microstructure of 304L stainless steel parts fabricated by laser-foil-printing additive manufacturing,” *The International*

Journal of Advanced Manufacturing Technology, vol. 112, no. 3, pp. 867–877, 2021, doi: 10.1007/s00170-020-06402-7.
[6] C.-H. Hung, A. Sutton, Y. Li, Y. Shen, H.-L. Tsai, and M. C. Leu, "Enhanced mechanical properties for 304L stainless steel parts fabricated by laser-foil-printing additive manufacturing," *J Manuf Process*, vol. 45, pp. 438–446, 2019, doi: https://doi.org/10.1016/j.jmapro.2019.07.030.
[7] Y. Li, Y. Shen, M. C. Leu, and H.-L. Tsai, "Building Zr-based metallic glass part on Ti-6Al-4V substrate by laser-foil-printing additive manufacturing," *Acta Mater*, vol. 144, pp. 810–821, 2018, doi: https://doi.org/10.1016/j.actamat.2017.11.046.
[8] Y. Li, Y. Shen, M. C. Leu, and H.-L. Tsai, "Mechanical properties of Zr-based bulk metallic glass parts fabricated by laser-foil-printing additive manufacturing," *Materials Science and Engineering: A*, vol. 743, pp. 404–411, 2019, doi: https://doi.org/10.1016/j.msea.2018.11.056.
[9] Y. Li, Y. Shen, C. Chen, M. C. Leu, and H.-L. Tsai, "Building metallic glass structures on crystalline metal substrates by laser-foil-printing additive manufacturing," *J Mater Process Technol*, vol. 248, pp. 249–261, 2017, doi: https://doi.org/10.1016/j.jmatprotec.2017.05.032.
[10] Y. Li, Y. Shen, C.-H. Hung, M. C. Leu, and H.-L. Tsai, "Additive manufacturing of Zr-based metallic glass structures on 304 stainless steel substrates via V/Ti/Zr intermediate layers," *Materials Science and Engineering: A*, vol. 729, pp. 185–195, 2018, doi: https://doi.org/10.1016/j.msea.2018.05.052.
[11] T. Turk, C.-H. Hung, M. H. Sehhat, and M. C. Leu, "Methods of Automating the Laser-Foil-Printing Additive Manufacturing Process," in *2021 International Solid Freeform Fabrication Symposium*, University of Texas at Austin, 2021, pp. 1142–1153. Accessed: Jun. 05, 2022. [Online]. Available: https://repositories.lib.utexas.edu/handle/2152/90714
[12] C.-H. Hung, T. Turk, M. H. Sehhat, and M. C. Leu, "Development and experimental study of an automated laser-foil-printing additive manufacturing system," *Rapid Prototyp J*, vol. 28, no. 6, pp. 1013–1022, Jan. 2022, doi: 10.1108/RPJ-10-2021-0269.
[13] T. Turk and M. C. Leu, "Experimental study for improving the productivity of laser foil printing," *The International Journal of Advanced Manufacturing Technology*, pp. 1–14, 2023, Accessed: Mar. 30, 2023. [Online]. Available: https://link.springer.com/article/10.1007/s00170-023-11076-y
[14] E. Manavalan and K. Jayakrishna, "A review of Internet of Things (IoT) embedded sustainable supply chain for industry 4.0 requirements," *Comput Ind Eng*, vol. 127, pp. 925–953, 2019, doi: https://doi.org/10.1016/j.cie.2018.11.030.
[15] P. M. Ferreira, M. A. Machado, M. S. Carvalho, and C. Vidal, "Embedded Sensors for Structural Health Monitoring: Methodologies and Applications Review," *Sensors*, vol. 22, no. 21, 2022, doi: 10.3390/s22218320.
[16] B.-H. Lu, H.-B. Lan, and H.-Z. Liu, "Additive manufacturing frontier: 3D printing electronics," *Opto-Electronic Advances*, vol. 1, no. 1, pp. 17000401–17000410, 2018, doi: 10.29026/oea.2018.170004.
[17] M. Binder, L. Kirchbichler, C. Seidel, C. Anstaett, G. Schlick, and G. Reinhart, "Design Concepts for the Integration of Electronic Components into Metal Laser-

based Powder Bed Fusion Parts," *Procedia CIRP*, vol. 81, pp. 992–997, 2019, doi: https://doi.org/10.1016/j.procir.2019.03.240.
[18] M. Binder, A. Machnik, M. Bosch, K. Kreitz, G. Schlick, and C. Seidel, "In-situ Integration of Weldable Strain Gauges in Components Manufactured by Laser-Based Powder Bed Fusion," in *2022 International Solid Freeform Fabrication Symposium*, University of Texas at Austin, 2022, pp. 1878–1894. Accessed: Mar. 27, 2023. [Online]. Available: https://repositories.lib.utexas.edu/handle/2152/117452
[19] S. M. Uí Mhurchadha, M. P. Huynh, P. T. Quinn, I. Tomaz, and R. Raghavendra, "A Methodology for the Embedding of Sensors in Components Manufactured Using Metal Laser Powder Bed Fusion," in *2021 International Solid Freeform Fabrication Symposium*, University of Texas at Austin, 2021.
[20] A. Mostafaei *et al.*, "Defects and anomalies in powder bed fusion metal additive manufacturing," *Curr Opin Solid State Mater Sci*, vol. 26, no. 2, p. 100974, 2022.
[21] L. Nuñez, P. Sabharwall, and I. J. van Rooyen, "In situ embedment of type K sheathed thermocouples with directed energy deposition," *The International Journal of Advanced Manufacturing Technology*, 2023, doi: 10.1007/s00170-023-11624-6.
[22] M. Juhasz *et al.*, "Hybrid directed energy deposition for fabricating metal structures with embedded sensors," *Addit Manuf*, vol. 35, p. 101397, 2020, doi: https://doi.org/10.1016/j.addma.2020.101397.
[23] T. Feldhausen *et al.*, "Embedding ceramic components in metal structures with hybrid directed energy deposition," *The International Journal of Advanced Manufacturing Technology*, vol. 125, no. 9, pp. 4425–4433, 2023, doi: 10.1007/s00170-023-10812-8.
[24] A. K. Ramanathan, M. B. Gingerich, L. M. Headings, and M. J. Dapino, "Metal structures embedded with piezoelectric PVDF sensors using ultrasonic additive manufacturing," *Manuf Lett*, vol. 31, pp. 96–100, 2022, doi: https://doi.org/10.1016/j.mfglet.2021.08.001.
[25] R. J. Friel and R. A. Harris, "Ultrasonic Additive Manufacturing – A Hybrid Production Process for Novel Functional Products," *Procedia CIRP*, vol. 6, pp. 35–40, 2013, doi: https://doi.org/10.1016/j.procir.2013.03.004.
[26] C. M. Jha, Ed., *Thermal Sensors*. New York, NY: Springer New York, 2015. doi: 10.1007/978-1-4939-2581-0.
[27] T. P. Wang, "Thermocouple Materials," in *Properties and Selection: Nonferrous Alloys and Special-Purpose Materials*, ASM International, 1990, pp. 869–888. doi: 10.31399/asm.hb.v02.a0001098.
[28] Z. Y. Chua, I. H. Ahn, and S. K. Moon, "Process monitoring and inspection systems in metal additive manufacturing: Status and applications," *International Journal of Precision Engineering and Manufacturing-Green Technology*, vol. 4, pp. 235–245, 2017.
[29] T. Liu *et al.*, "In-situ infrared thermographic inspection for local powder layer thickness measurement in laser powder bed fusion," *Addit Manuf*, vol. 55, p. 102873, 2022, doi: https://doi.org/10.1016/j.addma.2022.102873.
[30] B. Schoinochoritis, D. Chantzis, and K. Salonitis, "Simulation of metallic powder bed additive manufacturing processes with the finite element method: A critical

review," *Proc Inst Mech Eng B J Eng Manuf*, vol. 231, no. 1, pp. 96–117, 2017, doi: 10.1177/0954405414567522.
[31] M. R. Yavari, K. D. Cole, and P. Rao, "Thermal Modeling in Metal Additive Manufacturing Using Graph Theory," *J Manuf Sci Eng*, vol. 141, no. 7, Jul. 2019, doi: 10.1115/1.4043648.